Antibacterial Activity and Antistatic Composites of Polyester/Ag-SiO_2 Prepared by a Sol–Gel Method

Chin-San Wu, Hsin-Tzu Liao

Department of Chemical and Biochemical Engineering, Kao Yuan University, Kaohsiung County, Taiwan 82101, Republic of China

Received 6 February 2010; accepted 22 November 2010
DOI 10.1002/app.33823
Published online 16 March 2011 in Wiley Online Library (wileyonlinelibrary.com).

ABSTRACT: Poly(butylene adipate-*co*-terephthalate) (PBAT) composites containing silver-silica (Ag-SiO_2) were prepared using an *in-situ* sol–gel process. Maleic anhydride-grafted PBAT (PBAT-*g*-MA) and multihydroxyl-functionalized Ag-SiO_2 were used to improve the compatibility and dispersibility of Ag-SiO_2 within the PBAT matrix. The composites were characterized morphologically using transmission electron microscopy and chemically using Fourier transform infrared spectrometry. The existence of Ag-SiO_2 nanoparticles on the substrate was confirmed by the ultraviolet–visible absorption spectra. The antibacterial and antistatic properties of the composites were evaluated whether SiO_2 enhanced the electrical conductivity was tested as well as whether Ag enhanced the antibacterial activity of the PBAT-*g*-MA/SiO_2 or PBAT/SiO_2 composites. The PBAT-*g*-MA/SiO_2 or PBAT/SiO_2 composite that contained Ag had better antibacterial activity (more than 1.3-fold). The functionalized PBAT-*g*-MA/Ag-SiO_2 composite can markedly enhanced antibacterial and antistatic properties due to the carboxyl groups of maleic anhydride, which acted as coordination sites for the Ag-SiO_2 phase, allowing the formation of stronger chemical bonds. © 2011 Wiley Periodicals, Inc. J Appl Polym Sci 121: 2193–2201, 2011

Key words: antibacterial; silica; silver; sol–gel technique

INTRODUCTION

In the field of material science, synergistic combinations of polymers and ceramics via sol–gel processes have recently attracted a great deal of attention because of the potential for developing new materials with desired properties through manipulating structures at a molecular level.[1–10] These organic–inorganic hybrid materials may have a controllable combination of the benefits of polymers (such as flexibility and ease of processing) and those of ceramics or silver (such as antibacterial, optical, magnetic, and dispersion stability). Research on organic–inorganic composites has primarily focused on inorganic modification of an organic polymer dominant phase.[11,12] Specifically, the polymeric biomaterials commonly used in sol–gel-processed ceramics or Ag-reinforced polymers are glassy polymers, semicrystalline polymers, and other polymeric media, such as membranes.[13,14]

The microstructures and the properties of hybrid materials depend greatly on the particle size of the inorganic phase, the uniform distribution of the inorganic phase within the organic phase, and the interfacial force between the two phases. The formation of hydrogen or covalent bonds between the two phases is normally used to establish this interfacial force.[15,16] Hydrogen bonds may arise from the basic group of the hydrogen acceptor in the polymer and the hydroxyl group of the intermediate species from metal alkoxides. Alternatively, covalent bonds may form through dehydration of hydroxyl groups in the polymer with residual silica-hydroxide (Si—OH) groups in the silica (SiO_2) network. Ag is believed to be compatible with all of these antimicrobial methods and is widely used in medical and other kinds of materials due to its powerful antimicrobial activity; some researchers have focused on its use in the development of antibacterial surfaces.[17]

Nanotechnology has infiltrated the field of cell biology in the form of silver-silica (Ag-SiO_2). Ag-SiO_2 has many potential applications in electronics, biomedicine, and other fields.[18,19] With a view to further improving the antibacterial and electrical conductivity properties of the inorganic polymer hybrid, in this study, poly(butylene adipate-*co*-terephthalate) (PBAT) composites with Ag-SiO_2 were prepared by a sol–gel process. Formation and dispersion of the Ag-silica network in the PBAT matrix was achieved using a sol–gel method, in which the formation of inorganic phase was via an *in situ*

Correspondence to: C.-S. Wu (t50008@cc.kyu.edu.tw).
Contract grant sponsor: National Science Council (Taipei City, Taiwan, R.O.C.); contract grant number: NSC 99-2221-E-244-002.

© 2011 Wiley Periodicals, Inc.

polymerization of silica acid and silver nitrate ($AgNO_3$) in the presence of PBAT. In addition, a maleic anhydride-grafted version of PBAT (PBAT-*g*-MA) was also investigated, on the presumption that maleic anhydride groups on this PBAT copolymer would react with residual silanol groups of the SiO_2 network.

PBAT has good mechanical and optical properties,[20,21] resistance to fatigue and wear, and resistance to creep fracture. It is used extensively to produce films, fibers, and packaging materials. Composite PBAT fibers have led to the development of materials with additional functional properties, such as high electrical conductivity,[22] and antibacterial activity.[23,24] Self-sterilizing fabrics made with antibacterial PBAT fibers have potential benefits including reduced disease transfer in hospital populations and biowarfare protection.

This study focused on the effects of functionalized Ag-SiO_2 on the chemical properties and electrical conductivity of PBAT-based composite materials. To our knowledge, Ag-SiO_2 has not previously been systematically evaluated as a reinforcement material in PBAT for the production of antibacterial and antistatic composites.

EXPERIMENTAL

Materials

PBAT resins were purchased from BASF Corp. (Florham Park, NJ), and tetraethoxysilane (TEOS) was obtained from SMS, Merck Chemical Co. (Frankfurt, Germany); they were used as received. Lactic acid, maleic anhydride (MA), $AgNO_3$, and tetrahydrofuran (THF) were obtained from Aldrich Chemical (Milwaukee, WI). MA was purified before use by recrystallization from chloroform. Benzoyl peroxide (BPO, Aldrich Chemical) was used as a polymerization initiator and was purified by dissolution in chloroform and reprecipitation in methanol. Other reagents were purified using conventional methods.

Grafting reaction and percentage

Using BPO as the initiator, MA was grafted onto molten PBAT under a nitrogen atmosphere at 120°C ± 5°C with a mixer rotor speed of 60 rpm. A mixture of MA and BPO was added in four equal portions at 2-min intervals to the molten PBAT to allow grafting to take place. Preliminary experiments showed that reaction equilibrium was attained in less than 10 h. Thus, reactions were allowed to progress for 10 h under stirring at a rotor speed of 60 rpm. The grafted product (~ 4 g) was then dissolved in 200 mL of refluxing tetrahydrofuran at 50°C ± 2°C, and the hot solution was filtered through several layers of cheesecloth. The cheesecloth was washed with 600 mL acetone to remove the tetrahydrofuran-insoluble unreacted maleic anhydride, and the product remaining on the cheesecloth was dried in a vacuum oven at 80°C for 24 h. The tetrahydrofuran-soluble product in the filtrate was extracted five times using 600 mL cold acetone for each extraction. Subsequently, the grafting percentage was determined using a titration method.

The MA loading of the THF-soluble polymer was determined by titration and expressed as a grafting percentage. Approximately 2 g of copolymer was heated for 2 h in 200 mL of refluxing THF. This solution was then titrated immediately with 0.03*N* ethanolic potassium hydroxide (KOH), which had been standardized against a solution of potassium hydrogen phthalate, with a phenolphthalein indicator. The acid number and the grafting percentage were then calculated using the following equations.[25–27]

$$\text{Acid number(mg KOH/g)} = \frac{V_{KOH}(\text{mL}) \times C_{KOH}(\text{N}) \times 56.1}{\text{polymer(g)}} \quad (1)$$

$$\text{Grafting percentage}(\%) = \frac{\text{Acid number} \times 98.1}{2 \times 561} \times 100\% \quad (2)$$

For the determination of grafting percentage of MA onto PBAT, to eliminate the acid number from the carboxylic end groups of the PBAT polyester, the acid number for PBAT was determined and then subtracted this value from the acid number obtained from PBAT-*g*-MA. It was found that the grafting percentage of MA onto PBST was 1.12 wt % as benzoyl peroxide and MA loadings were 0.3 and 10 wt %, respectively.

Preparation of hybrids from PBAT, PBAT-*g*-MA, SiO_2, and Ag-SiO_2

A mixture called "Sol A" was prepared by dissolving a stoichiometric amount of TEOS, $AgNO_3$, H_2O, and lactic acid (a catalyst) in THF (Table I) and then stirring it at room temperature for 1 day to obtain a homogeneous solution. As shown in Table I, a predetermined amount of PBAT or PBAT-*g*-MA was put into a "Plastograph" 200 Nm Mixer W50EHT instrument (Brabender, Dayton, OH) with a blade-type rotor set at 50 rpm, and at a temperature of 120–130°C. When the polymer had melted completely, Sol A was added and the sol–gel process was allowed to proceed for 20 min. Prior to characterization, each sample was dried at 105°C in a vacuum oven for 3 days to remove residual solvent. Hybrid products were pressed into thin plates using a hot press at 130°C and then put into a dryer for

TABLE I
Compositions of Various Sol–Gel Liquid Solutions for the Preparation of Hybrid Materials

SiO_2 (wt %)	5	10	10
PBAT or PBAT-*g*-MA (g)	36.26	30.77	30.77
TEOS (g)	6.56	11.89	11.89
Sol A			
THF (g)	6.56	11.89	11.89
[lactic acid]/[TEOS][a]	0.01	0.01	0.01
[H_2O]/[TEOS][a]	2.2	2.2	2.2
[$AgNO_3$]/[TEOS][a]	–	–	0.02

[a] The mole ratio of lactic acid, H_2O, and $AgNO_3$ to TEOS.

cooling, after which they were made into standard specimens for characterization.

Characterization of hybrid composites

Fourier transform infrared spectrometry (FTIR; FTS-7PC type; Bio-Rad, Hercules, CA) was used to investigate the grafting reaction of MA onto PBAT and to verify ester bond formation between the sol–gel Si—OH phase and the PBAT matrix. Samples subjected to FTIR analysis were ground into fine powders in a milling machine and pressed into pellets with potassium bromide. Ultraviolet–visible (UV–vis) absorption spectra were recorded on a UV2001-PC spectrophotometer (Hitachi, Tokyo, Japan). To obtain transmission electron micrographs, samples were mounted in epoxy resin and the Ag-SiO_2 was cut with a microtome to create specimens 60–100 nm thick. Micrographs were acquired with a transmission electron microscope (JEM-100CX II; JEOL, Tokyo, Japan) at an acceleration voltage of 100 kV. The X-ray diffraction intensity curves were recorded with Rigaku D/max 3V X-ray diffractometer, using Cu Kα radiation with a scanning rate 2°/min, to study the particle size of Ag. Electrical resistivity was measured directly on laminated films (0.1 mm thick) with an Ohm-Stat RT-1000 Standard Resistivity Tester (Static Solutions, USA).

Determination of antibacterial properties

E. coli, which is widely used as a biological index for pollution and contamination in water and instrumentation, was chosen as the standard bacterium for determining the antibacterial properties of the composite materials. *E. coli* (BCRC 10239) was obtained from the Bioresource Collection and Research Center (BCRC; Hsinchu, Taiwan) and was maintained in nutrient broth (NB) medium. The NB medium consisted of 3 g of beef extract and 5 g of peptone in 1 L of distilled water at pH 7.0. The pH of the medium was controlled by adjusting with 1*N* NaOH solutions. Nutrient agar was produced with the addition of 15 g of agar to 1 L of NB. The bacteria were stored at −20°C in NB medium containing 60% glycerol. Prior to testing, 150 mL of NB medium was inoculated with a 10-μL aliquot of preserved bacteria, and the culture was grown aerobically at 35°C. After overnight incubation, 3 mL of the bacterial solution was transferred to fresh NB medium and then kept at 35°C under shaking at 120 rpm for 18 h. A well was constructed (3.00 cm diameter and 0.03 cm thick) on the surface of each sample (5.00 cm diameter and 0.10 cm thickness) to hold the bacterial suspension in contact with the composite sample. A 0.02-mL aliquot of bacterial suspension ($1.3 \pm 0.3 \times 10^6$ colony-forming units [CFUs]/mL) was placed on the surface of each sample and covered with a germless polyethylene film [4.00 cm diameter and 0.05 cm thick; Fig. 1(A)]. The samples were incubated at 35°C ± 1°C at a relative humidity of approximately 90%. After incubation, samples were washed with 1.98 mL of NaCl solution (0.85%) for 3–24 h. The washing solution was diluted 10^5 with NaCl solution, and 20-μL aliquot of diluted solution was separated on NB agar medium. After incubation for 24 h, the number of CFUs of *E. coli* was determined by direct plate counting.

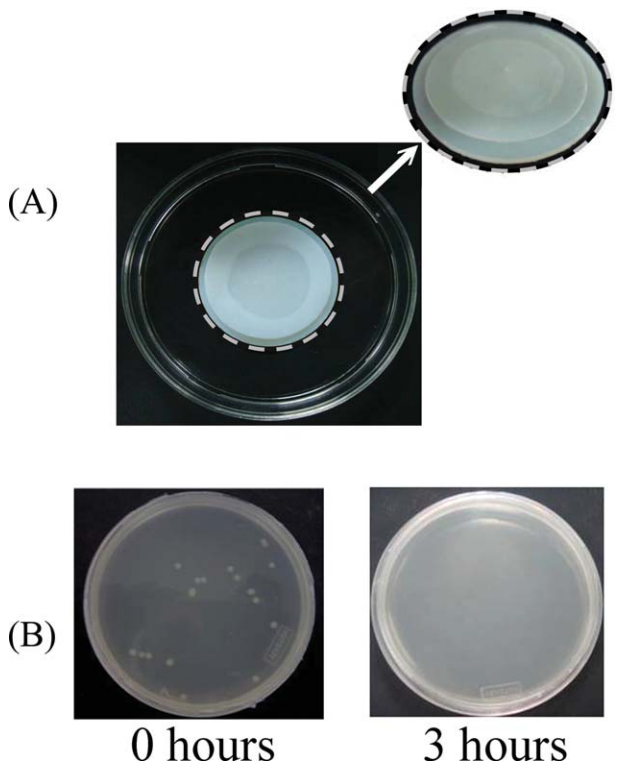

Figure 1 (A) Photographs show PBAT-*g*-MA/Ag-SiO_2 (10 wt %) samples loaded with a fixed volume (0.1 mL) of *E. coli*. (B) *E. coli* was exposed to PBAT-*g*-MA/Ag-SiO_2 (10 wt %) to evaluate antibacterial activity. [Color figure can be viewed in the online issue, which is available at wileyonlinelibrary.com]

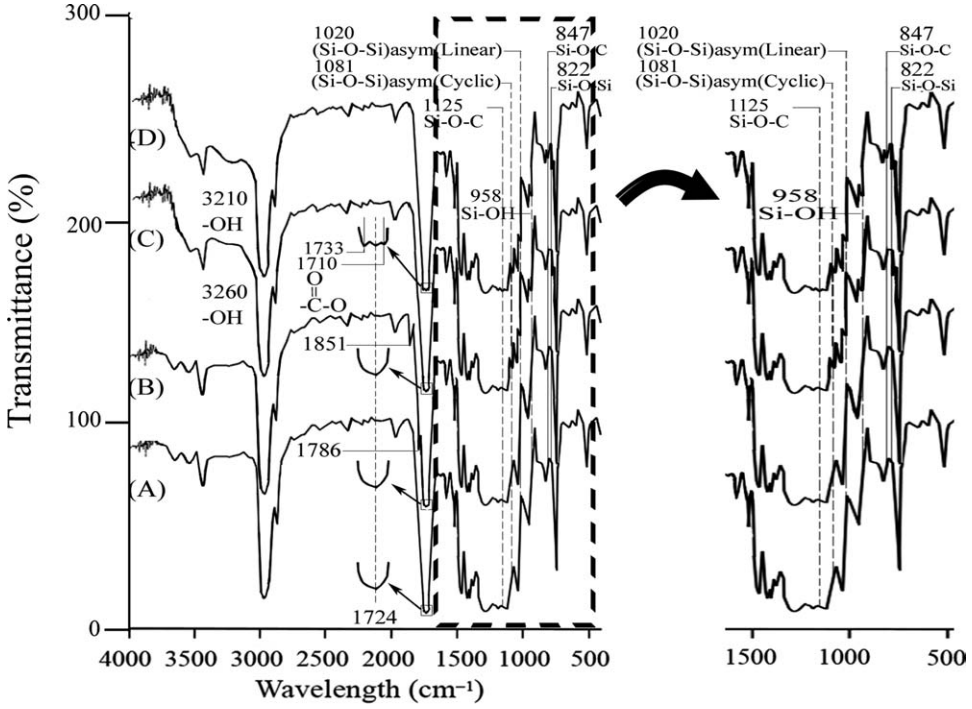

Figure 2 FTIR spectra of (A) PBAT, (B) PBAT-*g*-MA, (C) PBAT/Ag-SiO_2 (10 wt %), and (D) PBAT-*g*-MA/Ag-SiO_2 (10 wt %).

Analysis of antibacterial capacity

The survival rate of bacteria exposed to the composite material was used to determine the antibacterial capacity of PBAT and its composites or PBAT-*g*-MA and its composites. The survival rate of bacteria was defined by the following equation:

$$\text{Survival rate} = \frac{y}{x} \times 100\%, \tag{3}$$

where x and y are the CFU counts before and after exposure. Figure 1(B) shows photographs of *E. coli* colonies from PBAT-*g*-MA/Ag-SiO_2 (10 wt %) samples that had been exposed to the composite for 3 h. The survival rate of *E. coli* was calculated using Eq. (3). Almost no *E. coli* had survived.

JISL 1902–1998, a method typically used to estimate drug toxicity, can also be applied to determining the antibacterial activity of Ag-SiO_2 composites. This method determines an antibacterial index (ABI) and kill-bacterial index (KBI) according to the following expressions:

$$ABI = \log B - \log C, \tag{4}$$

$$KBI = \log A - \log C, \tag{5}$$

where A is the number of bacteria recovered from the inoculated, untreated sample (native PBAT or PBAT-*g*-MA) immediately following inoculation; B is the number of bacteria remaining in the inoculated, untreated sample after 18 h; and C is number of bacteria remaining in the inoculated, treated sample after 18 h. According to the antibacterial standard of the Japanese Association for the Functional Evaluation of Textiles, an ABI greater than 2.2 indicates bacterial inhibition, and a KBI greater than 0 indicates a bactericidal effect.

RESULTS AND DISCUSSION

Infrared spectroscopy

The FTIR spectra of unmodified PBAT and PBAT-*g*-MA are shown in Figure 2(A,B), respectively. The characteristic transitions of PBAT.[28] at 3300–3700, 1700–1760, and 500–1500 cm^{-1} appeared in the spectra of both polymers, with two extra shoulders observed at 1786 and 1851 cm^{-1} in the modified PBAT spectrum. These features are characteristic of anhydride carboxyl groups. Similar results have been reported previously.[29,30] The extra shoulders that appear at 1786 and 1851 cm^{-1} are due to the vibration of anhydride carbonyl group of MA grafted in PBAT and thus indicate the grafting of MA onto PBAT.

New peaks, at about 3000–3600 and 700–1800 cm^{-1}, appeared in the FTIR spectrum of the PBAT/Ag-SiO_2 (10 wt %) and PBAT-*g*-MA/Ag-SiO_2 (10 wt %) composites [Fig. 2(C,D)]. The broad peak at about 3000–3600 cm^{-1} in the spectra of PBAT/Ag-SiO_2 (10 wt %) and PBAT-*g*-MA/Ag-SiO_2 (10 wt %) is due to the presence of O—H groups (Si—OH) and the formation of hydrogen bonds, while the peaks in the

range 700–1800 cm^{-1} indicate the SiO_2 phase. The peaks at 700–1800 cm^{-1} are the result of a Si—O—Si (1020 and 1081 cm^{-1}) bond. The observed stretching vibration of $(Si—O—Si)_{asym}$ (asymmetric) at 1000–1100 cm^{-1} [Fig. 2(C,D)] represents condensation reactions between Si—OH groups. Notably, the $(Si—O—Si)_{asym}$ vibration consists of two components arising from Si—O—Si groups in linear fragments ($\sim$ 1021 cm^{-1}) and in loops ($\sim$ 1081 cm^{-1}) (indicated as "cyclic" in Fig. 2).[31] Consequently, a comparison of linear and cyclic components' absorbance magnitudes contributes to understanding the degree of molecular connectivity within the silicon oxide phase. Meanwhile, the Si—OH vibration absorbance ($\sim$ 958 cm^{-1}) is a measure of the number of uncondensed silanol groups. Thus, the relative absorbance of these two types of bands (Si—O—Si and Si—OH) allows an assessment of the degree of crosslinking within the incorporated silicon oxide phases. Another signature of network-forming in the Ag-SiO_2 phase is a peak at around 822 cm^{-1}, representing symmetric vibration of Si—O—Si groups ($[Si—O—Si]_{sym}$). Although the symmetric vibration of Si—O—Si is theoretically FTIR-inactive, its presence is attributable to distortion of bonding symmetry about the tetrahedral SiO_4. Comparing the spectra of PBAT-*g*-MA and PBAT-*g*-MA/Ag-SiO_2 [10 wt %; Fig. 2(B,D)], one can see peaks at 1786 and 1851 cm^{-1} in the former. These are not present in the latter; two new peaks at 1733 and 1716 cm^{-1} are detected, and the absorbance at 847 and 1125 cm^{-1} is caused by a Si—O—C group. They may be due to the formation of ester groups through the reaction between anhydride carboxyl groups of PBAT-*g*-MA and Si—OH groups of the Ag-SiO_2 network.[32]

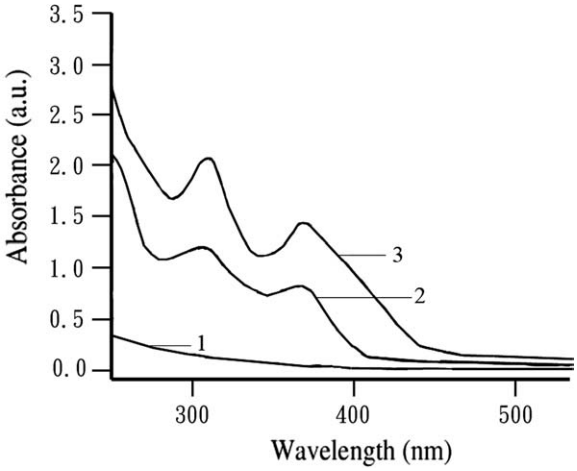

Figure 3 Absorption spectra of (1) Ag-SiO_2, (2) PBAT/Ag-SiO_2 (10 wt %), and (3) PBAT-*g*-MA/Ag-SiO_2 (10 wt %) in a THF solution after 50 min.

UV–vis analysis

To further demonstrate the covalent linkage between PBAT-*g*-MA and Ag-SiO_2, the dispersibility of the materials in THF was evaluated. The immobilization of Ag nanoparticles throughout the Ag-SiO_2 hydrogel networks is due to a strong localization of particles within the gel networks. The formation of Ag nanoparticles in the Ag-SiO_2 hydrogel networks may be due to the adsorption of Ag nanoparticles through nitrogen atoms and/or oxygen atoms present in the Ag-SiO_2 hydrogel macromolecular chains. The presence of embedded Ag nanoparticles within the gel macromolecular networks was confirmed by UV–vis spectral studies. Conversely, the hydrophobic polymer chains of PBAT-*g*-MA/Ag-SiO_2 were soluble in THF.

In situ UV–vis absorbance spectra and digital photographs of PBAT/Ag-SiO_2 (10 wt %), PBAT-*g*-MA/Ag-SiO_2 (10 wt %), and Ag-SiO_2 placed in THF solution are shown in Figure 3. The insolubility of Ag-SiO_2 in THF is evident in line 1, which shows almost no absorption from 300 to 500 nm. Both PBAT/Ag-SiO_2 and PBAT-*g*-MA/Ag-SiO_2 were increasingly soluble in the THF phase due to increased binding between PBAT and Ag-SiO_2 or PBAT-*g*-MA and Ag-SiO_2. Apparent absorbance was observed at around 311 (Ag) and 367 nm (relatively broad band) for these composites (lines 2 and 3 in Fig. 3). Moreover, the PBAT/Ag-SiO_2 (10 wt %) samples contained more precipitate and exhibited a lower absorbance than samples of PBAT-*g*-MA/Ag-SiO_2 (10 wt %). The presence of covalent links between constituents likely enhanced the dispersibility of PBAT-*g*-MA/Ag-SiO_2 (10 wt %) versus that of PBAT/Ag-SiO_2 (10 wt %).

Hybrid morphology

The morphology of the SiO_2 or Ag-SiO_2 and polymer composites may be directly related to their electrical properties. In general, good dispersion of SiO_2 or Ag-SiO_2 throughout the polymer matrix, effective functionalization of SiO_2 or Ag-SiO_2, and strong interfacial adhesion between the two phases are required to obtain a composite material with satisfactory electrical and antibacterial properties. Tensile fractured surfaces of PBAT/SiO_2 and PBAT-*g*-MA/Ag-SiO_2 composites were imaged by transmission electron microscopy (TEM). In general, individual embedded Ag-SiO_2 was difficult to locate in samples exhibiting sufficient dispersion and good interfacial adhesion between Ag-SiO_2 and the polymer matrix.[33,34] Using the sol–gel method proposed in this study, as the comparison between Figure 4(A,B), the images of the TEM analysis indicate that the Ag particles were embedded within the SiO_2 matrix anddeposited on the surface. From Figure 4(B), it

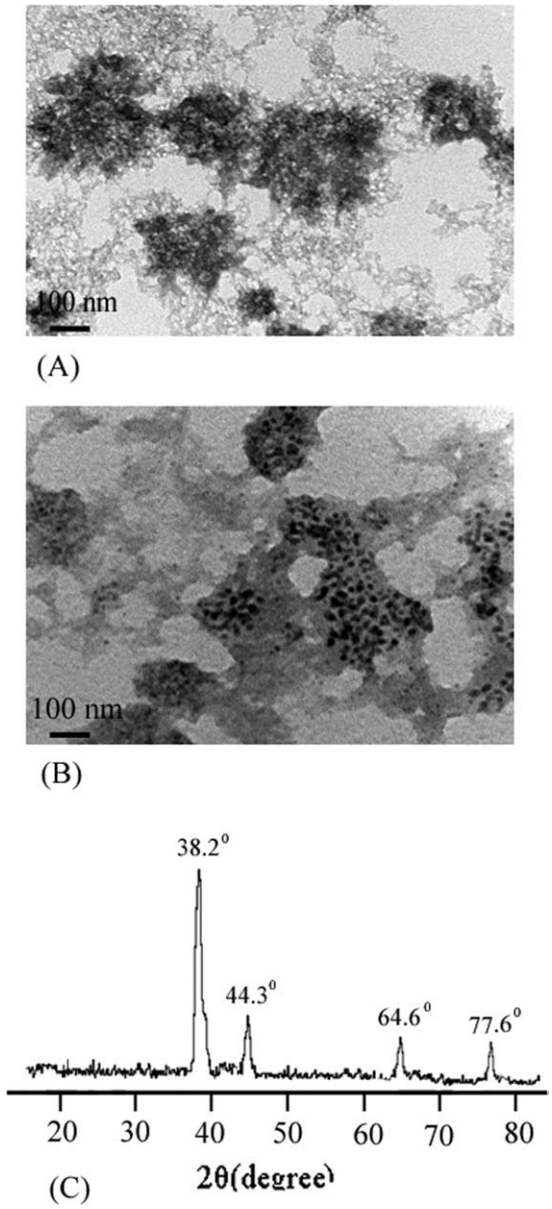

Figure 4 TEM and XRD pattern of composites (A) PBAT-*g*-MA/SiO_2 (10 wt %); (B) PBAT-*g*-MA/Ag-SiO_2 (10 wt %), and (C) PBAT-*g*-MA/Ag-SiO_2 (10 wt %) composites.

can be observed that the sizes of Ag particles are in the range 10–35 nm. To further confirm the particle size of Ag obtained from TEM, it is also studied by the XRD analysis. It can be observed from Figure 4(C) that the XRD pattern of the PBAT-*g*-MA/Ag-SiO_2 composite gives the significant characteristic peaks of 38.2°, 44.3°, 64.6°, and 77.6°. By using the Scherrer equation, the particle size of Ag is about 31.3 nm,[35] which is consistent with the result obtained from TEM image. Thus, the result that PBAT-*g*-MA/Ag-SiO_2 composites have better antibacterial activity may be due to the distribution of Ag in SiO_2 and is discussed in more detail in the following sections.

Electrical properties

The electrical resistivity of PBAT ($\sim 10^{16}$ Ω/sq) and its composites or PBAT-*g*-MA ($\sim 10^{16}$ Ω/sq) and its composite hybrid materials are summarized in Figure 5. A marked decrease was observed in electrical resistivity with increasing SiO_2 content to 5 wt % (8.1×10^9 to 7.3×10^{10} Ω/sq), above which the electrical resistivity decreased. When the content of SiO_2 was 10 wt %, the electrical resistivity decreased to 7.5×10^8 to 4.1×10^9 Ω/sq, and the downside of electrical resistivity was more moderate. When the content of Ag-SiO_2 was 10 wt % in PBAT or PBAT-*g*-MA composites, the electrical resistivity was about 8.4×10^7 to 4.6×10^8 Ω/sq. Thus, these results suggest that the decrease in electrical resistivity of PBAT and its composites or PBAT-*g*-MA and its composites were due to the content of SiO_2 and Ag-SiO_2, and when the content was equal (10 wt %), the electrical resistivity of PBAT/Ag-SiO_2 and PBAT-*g*-MA/Ag-SiO_2 was almost the same.

The reduced electrical resistivity of PBAT-*g*-MA/Ag-SiO_2 was likely caused by inhibited polymer motion, which would have prohibited the chain rearrangement and reorganization required for solidification. As expected, both PBAT/Ag-SiO_2 and PBAT-*g*-MA/Ag-SiO_2 exhibited lower electrical resistivity than pure PBAT and PBAT-*g*-MA. The decrease in electrical resistivity was greater in PBAT-*g*-MA/Ag-SiO_2 than in PBAT/Ag-SiO_2, presumably due to ester bond formation, as previously discussed. Ester linkages are stronger than the hydrogen bonds formed in PBAT/Ag-SiO_2 and therefore are more effective in hindering polymer motion. Moreover, the electrical resistivity of all PBAT-*g*-MA/Ag-SiO_2 hybrids was lower than that of their PBAT/Ag-SiO_2 equivalents.

Although the 10% PBAT/Ag-SiO_2 and PBAT-*g*-MA/Ag-SiO_2 composites exhibited resistivity values as low as 4.6×10^8 and 8.4×10^7 Ω/sq, respectively,

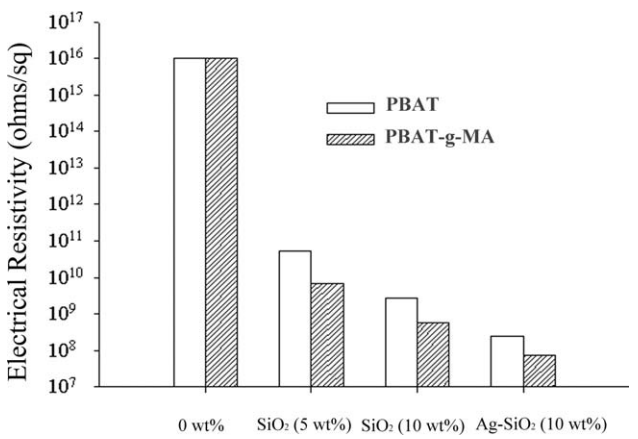

Figure 5 Electrical resistivity of PBAT, PBAT-*g*-MA, PBAT/SiO_2, and PBAT-*g*-MA/Ag-SiO_2 composites.

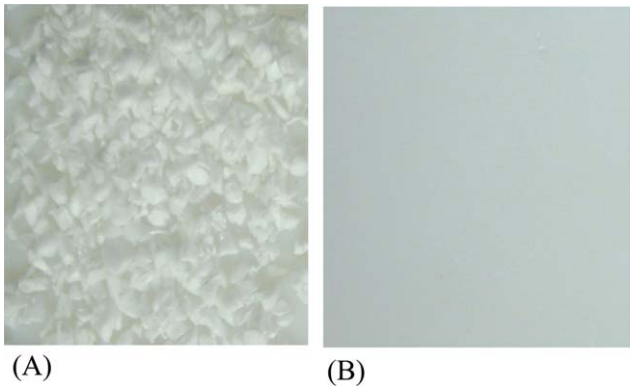

Figure 6 Antistatic properties of (A) PBAT-*g*-MA and (B) PBAT-*g*-MA/Ag-SiO$_2$ (10 wt %). [Color figure can be viewed in the online issue, which is available at wileyonlinelibrary.com]

they cannot be classified as "conductive materials." They can, however, be referred to as "antistatic materials." According to the standards of the Electronic Industry Association, a surface resistivity of less than 1.0×10^5 Ω/sq is required for a material to be classified as "conductive." Surface resistance values of "dissipative materials" range from 1.0×10^5 to 1.0×10^{12} Ω/sq, and the surface resistivity of "insulative materials" must be 1.0×10^{12} Ω/sq.[36] Figure 6 shows the results of antistatic testing with pristine PBAT-*g*-AA and 10% PBAT-*g*-MA/Ag-SiO$_2$ (sample size: $5.0 \times 5.0 \times 0.1$ cm^3). Each film was rubbed and immersed in small plastic foam balls. Any adsorption of plastic balls would indicate the presence of static electricity. The pristine PBAT-*g*-MA adsorbed a significant number of plastic balls, whereas the 10% PBAT-*g*-MA/Ag-SiO$_2$ composite was clean. Thus, the addition of Ag-SiO$_2$ to the composite resulted in electrostatic dissipative properties in the bulk material.

Antibacterial properties of composites

Antibacterial activity was evaluated with clinical infectious *E. coli*. ABI and KBI values were calculated according to JISL 1902–1998 and are presented in Table II. As shown in Figure 7(A), the *E. coli* cell

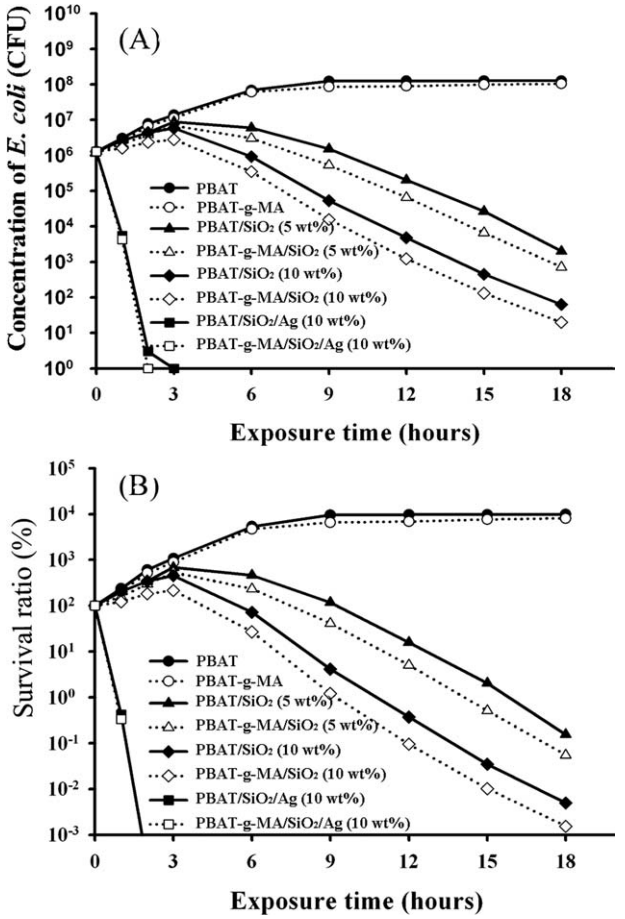

Figure 7 Exposure time course growth (A) *E. coli* cells and (B) of survival ratio during exposure to PBAT or PBAT-*g*-MA and its composite surfaces.

count increased with time, from 1.30×10^6 to 1.28×10^8 CFU mL^{-1} or from 1.30×10^6 to 1.05×10^8 CFU mL^{-1}, respectively, after incubation at 37°C for 24 h, when in contact with PBAT or PBAT-*g*-MA. Conversely, under the same conditions, the bacterial cell count decreased rapidly to near zero when in contact with PBAT/SiO$_2$ or PBAT-*g*-MA/SiO$_2$ containing more than 10 wt % SiO$_2$. At 10 wt % SiO$_2$, the onset of *E. coli* reduction was observed at 6 h. However, the onset of *E. coli* reduction was observed at 1 h when the content of Ag-SiO$_2$ was 10 wt %. From the results in Table I and the guidelines set

TABLE II
The Antibacterial Properties of PBAT/SiO$_2$ (10 wt %), PBAT-*g*-MA/SiO$_2$ (10 wt %), PBAT/Ag-SiO$_2$(10 wt %), and PBAT-*g*-MA/Ag-SiO$_2$ Composites

Composites	PBAT/SiO$_2$ (10 wt %)	PBAT-*g*-MA/SiO$_2$ (10 wt %)	PBAT/Ag-SiO$_2$ (10 wt %)	PBAT-*g*-MA/Ag-SiO$_2$ (10 wt %)
A (CFU/mL^{-1})	1.30×10^6	1.30×10^6	1.30×10^6	1.30×10^6
B (CFU/mL^{-1})	1.28×10^8	1.28×10^8	1.28×10^8	1.28×10^8
C (CFU/mL^{-1})	6.40×10^1	2.00×10^1	0	0
ABI	6.30	6.81	>8.11	>8.11
KBI	4.31	4.81	>6.11	>6.11

forth by JISL 1902–1998 and the Japanese Association for the Functional Evaluation of Textiles, one can conclude that PBAT-*g*-MA/SiO_2 and PBAT-*g*-MA/Ag-SiO_2 suppress the growth of *E. coli*. All of the samples of PBAT-*g*-MA/Ag-SiO_2 exhibited a higher degree of bacterial suppression than the corresponding samples of PBAT-*g*-MA/SiO_2 or PBAT/SiO_2. This is a result of ester formation from condensation of the carboxylic acid groups of PBAT-*g*-MA with the hydroxyl groups of Ag-SiO_2.

Figure 7(B) shows that the survival ratio of *E. coli* in contact with PBAT or PBAT-*g*-MA increases with time up to 12 h, when an equilibrium was reached. In contrast, the survival ratio of *E. coli* in contact with PBAT-*g*-MA/SiO_2 or PBAT/SiO_2 began to decrease after only 6 h. Thus, composite materials with SiO_2 suppressed the growth of *E. coli*. Composites containing more than 10 wt % SiO_2 showed a rapid decrease in the survival ratio in the first 18 h and a slower decline thereafter. The survival ratio for both PBAT-*g*-MA/SiO_2 and PBAT/SiO_2, which inversely indicates the extent of antibacterial activity, decreased as the content of SiO_2 increased. The PBAT-*g*-MA/SiO_2 composites consistently yielded a lower survival ratio than the PBAT/SiO_2 composites. The higher antibacterial activity of PBAT-*g*-MA/SiO_2 may be a result of electrostatic interactions. Bacterial strains, such as *E. coli*, with an extracellular capsule, carry less negative charge and are less prone to adsorption on the positively charged surface of PBAT-g-MA/SiO_2. However, the composites of PBAT-*g*-MA/SiO_2 or PBAT/SiO_2 that contained Ag had better antibacterial activity (more than 1.3-fold).

CONCLUSIONS

In this article, organic–inorganic hybrid materials were prepared using an *in situ* sol–gel process. FTIR showed that the maleic anhydride had been grafted onto the PBAT copolymer and that Si—O—Si and Si—O—C bonds had formed in the PBAT-*g*-MA/Ag-SiO_2 hybrid. The newly formed Si—O—C and bonds may be produced through dehydration of maleic anhydride groups in the PBAT-*g*-MA matrix with residual Si—OH groups in the Ag-SiO_2 network. The existence of Ag-SiO_2 nanoparticles on the substrate was also confirmed by UV–vis spectroscopy. Apparent absorbance was observed at around 311 (Ag) and 367 nm (relatively broad band) with these composites. Transmission electron micrographs of the composites showed the formation of Ag-SiO_2. The electrical resistivity of the PBAT-*g*-MA/Ag-SiO_2 (10 wt %) composite was 8.4×10^7 Ω/sq, which is 10^8-fold lower than that of neat PBAT, which afforded a high antistatic efficiency. According to the antibacterial capacity evaluation, PBAT-*g*-MA/Ag-SiO_2 composite film had a zone of bacteria growth inhibition around the samples, but PBAT-*g*-MA and PBAT-*g*-MA/SiO_2 composite films did not. Materials that contained Ag had strong antibacterial effects. Antibacterial activity was enhanced with the addition of 10 wt % Ag-SiO_2 to PBAT-*g*-MA, resulting in ABI and KBI values of more than 8.11 and 6.11, respectively. Thus, this study demonstrates an enhancement in compatibility between PBAT and Ag-SiO_2, with antibacterial and antistatic properties.

References

1. Kamperman, M.; Fierke, M. A.; Garcia, C. B. W.; Wiesner, U. Macromolecules 2008, 41, 8745.
2. Gill, I. Chem Mater 2001, 13, 3404.
3. Mackenzie, J. D.; Bescher, E. P. Acc Chem Res 2007, 40, 810.
4. Huang, L. P. Q.; Liu, B.; Bando, Y.; Hsieh, Y. L.; Mukherjee, A. K. J Am Chem Soc 2009, 131, 10346.
5. Zheludkevich, M. L.; Shchukin, D. G.; Yasakau, K. A.; Möhwald, H.; Ferreira, M. G. S. Chem Mater 2007, 19, 402.
6. Mutin, P. H.; Vioux, A. Chem Mater 2009, 21, 582.
7. Kartsonakis, I. A.; Liatsi, P.; Daniilidis, I.; Kordas, G. J Am Ceram Soc 2008, 91, 372.
8. Thiel, J.; Pakstis, L.; Buzby, S.; Raffi, M.; Ni, C.; Pochan, D. J.; Shah, S. I. Small 2007, 3, 799.
9. Rhee, S. H.; Choi, J. Y.; Kim, H. M. Biomaterials 2002, 23, 4915.
10. Balamurugana, A.; Balossierb, G. D.; Pinaa, L. M. S.; Rebeloa, A. H. S.; Faureb, J.; Ferreiraa, J. M. F. Dent Mater 2008, 24, 1343.
11. Poovarodom, S.; Hosseinpour, D.; Berg, J. C. Ind Eng Chem Res 2008, 47, 2623.
12. Marini, M.; Niederhausern, S. D.; Iseppi, R.; Bondi, M.; Sabia, C.; Toselli, M.; Pilati, F. Biomacromolecules 2007, 8, 1246.
13. Ji, Q.; Wang, X.; Zhang, Y.; Kong, Q.; Xia, Y. Comp Part A Appl Sci Manuf 2009, 40, 878.
14. Lin, C. H.; Chang, C. H.; Jao, W. C.; Yang, M. C. Polym Adv Technol 2009, 20, 672.
15. Lin, C. L.; Yeh, M. Y.; Chen, C. H.; Sudhakar, S.; Luo, S. J.; Hsu, Y. C.; Huang, C. Y.; Ho, K. C.; Luh, T. Y. Chem Mater 2006, 18, 4157.
16. Liu, R.; Shi, Y.; Wan, Y.; Meng, Y.; Zhang, F.; Gu, D.; Chen, Z.; Tu, B.; Zhao, D. J Am Chem Soc 2006, 128, 11652.
17. Jeon, H. J.; Yi, S. C.; Oh, S. G. Biomaterials 2003, 24, 4921.
18. Han, C.; Bian, J.; Liu, H.; Dong, L. Polym Int 2009, 58, 691.
19. Glenn, G.; Klamczynski, A.; Ludvik, C.; Chiou, B. S.; Imam, S.; Shey, J.; Orts, W.; Wood, D. Pack Technol Sci 2007, 20, 77.
20. Zou, H.; Wu, S.; Shen, J. Chem Rev 2008, 108, 3893.
21. Tomšič, B.; Simončič, B.; Orel, B.; Žerjav, M.; Schroers, H.; Simončič, A.; Samardžija, Z. Carbohydr Polym 2009, 75, 618.
22. Marini, M.; Niederhausern, S. D.; Iseppi, R.; Bondi, M.; Sabia, C.; Toselli, M.; Pilati, F. Biomacromolecules 2007, 8, 1246.
23. Lv, Y.; Liu, H.; Wang, Z.; Hao, L.; Liu, J.; Wang, Y.; Du, G.; Liu, D.; Zhan, J.; Wang, J. Polym Adv Technol 2008, 19, 1455.
24. Tian, C.; Mao, B.; Wang, E.; Kang, Z.; Song, Y.; Wang, C.; Li, S. J Phys Chem C 2007, 111, 3651.
25. Wu, C. S. Polym Degrad Stabil 2003, 80, 127.
26. Gaylord, N. G.; Mehta, R.; Kumar, V.; Tazi, M. J Appl Polym Sci 1989, 38, 359.
27. Martinez, J G.; Benavides, R.; Guerrero, C.; Reyes, B. E. Polym Degrad Stabil 2004, 86, 129.
28. Raquez, J. M.; Nabar, Y.; Narayan, R.; Dubois, P. Polym Eng Sci 2008, 48, 1747.

29. Nakason, C.; Kaesaman, A.; Supasanthitikul, P. Polym Test 2004, 23, 35.
30. Sclavons, M.; Laurent, M.; Devaux, J.; Carlier, V. Polymer 2005, 46, 8062.
31. Shao, P. L.; Mauritz, K. A.; Moore, R. B. J Polym Sci B: Polym Phys 1996, 34, 873.
32. Wu, C. S.; Liao, H. T. J Polym Sci B Polym Phys 2003, 41, 351.
33. Jeong, H. S.; Hoy, Y. P.; Dong, P. K.; Dong, S. B. Colloids Surf A Physicochem Eng Asp 2008, 313–314, 105.
34. Leite, E. R.; Carreno, N. L. V.; Longo, E.; Pontes, F. M. Chem Mater 2002, 14, 3722.
35. Kang, H.; Zhu, Y.; Jing Y.; Yang X.; Li, C. Colloids Surf A Physicochem Eng Asp 2010, 356, 120.
36. Narkis, M.; Lidor, G.; Vaxman, A.; Zuri, L. J Electrostat 1999, 47, 201.